Photometric and Radiative Transfer Analysis of the Temporal Variations of Aerosol Characteristics over Singapore

PC4199 Honours Project in Physics, Final Report
Department of Physics
Academic Year 2016/2017

Submitted by:

Yap Jin Min Ruth
A0115322X

Supervisors:

Dr Santo V. Salinas Cortijo

Dr Liew Soo Chin

Abstract

The optical properties of aerosols determine their effects on the Earth's radiation and heat budget. Though the number of aerosol studies have increased over the years, their impact on climate is still not well-understood. In this study, we perform a photometric and radiative transfer analysis of aerosol characteristics over Singapore, using data from 2006 to 2016, to understand how dominant aerosol species (urban pollutants and biomass burning smoke) affect the local climate. The aerosol parameters – Aerosol Optical Depth and the Angstrom Exponent number – were retrieved from the Aerosol Robotic Network (AERONET), and a statistical analysis on the temporal variations performed. Computation of the aerosol radiative forcing was conducted using the Langley Fu and Liou Radiative Transfer model. The analyses show that biomass burning aerosols have seasonal occurrence during the Southwest Monsoon, while urban pollutants are present all year round. There is a clear growing time of influence of both smoke and urban pollution particulates, and a reduction in aerosol particle size across the ten years of study. Aerosol inputs reported consistent net cooling effects; the seasons with transboundary smoke recording a radiative forcing of greater magnitude than those seasons without. However, only the direct impacts of aerosols on climate have been explored. The indirect impacts, motivated by known feedback mechanisms between clouds and aerosols, would greatly enhance the understanding of aerosols' climatic effects.

Preface

SINGAPORE. I think back to a day some 3.5 years back. The opening of my front door sends a gush of unfamiliarity into my face. My eyes tear up. My nose tickles. I hear stale silence in a habitually chirpy HDB estate. The block opposite mine looks as though it became a murky yellow overnight. Straight lines and edges don't quite look as defined as I am accustomed to. Another step out chokes me up. I want to turn back, shut the door and lock myself up again, but commitment calls me to trudge my feet out the house. It's Friday, but the end-of-the-week hype is felt only remotely. For all the wrong reasons, it is a day to keep in remembrance.

The date is 21 June 2013.

The PSI is 401.

Acknowledgements

I've been blessed to have Dr Santo Salinas as my supervisor: for his overwhelming emphasis on my learning over actual results; for his patience in taking me through all the theory, math and processing and breaking them down into simple, digestible steps to follow; for him availing himself to help anytime I needed. The journey has been a memorable one for these things. I'm thankful also to Dr Liew, for giving me this chance to learn at CRISP and stirring my interest in remote sensing, and to the other staff and research scientists whose greetings and concern made the hours in the cold research laboratory much more bearable. Dr Liew and Dr Santo are also the principal investigators of the Singapore AERONET site, from which the data in the following report has been retrieved.

Thank you to all my professors, lecturers and tutors during my time in NUS, for patiently teaching an oddball like me. I thought I'd be judged in some way for being here studying Physics and yet always thinking about pursuing paths in completely unrelated things. Still, you each continued to nurture, doing whatever it took for me to get through your module, and expressed a genuine interest in my unusual dreams, the whole time without treating me any differently. AHA moments didn't always come by, but when they did I knew it was because you worked doubly hard to understand things from my level and built the foundation from there. Thank you for living out the heart of what it means to be an educator and for reminding me of why I first started out on this foray into Physics in the first place.

For the individuals I got to know in the Navigators, the fellowship we share has been one of God's greatest gifts to me in this season. If I could ever go back to 4 years ago and have the options laid before me again, I would still choose to be here. Your exemplary lives have challenged me to make these years count for something more than just a degree. Thank you for your encouragement, prayers

and companionship. Thank you, Rachel, for every moment you committed to journey with me – in laughter, in tears, in worry or just plain "sian-ness".

To my family – Daddy, Mummy and Buddy – thank you for putting up with my rollercoaster emotions. I imagine it would have been hard living with a sluggish grouch in one moment and then a whiny, hyperactive 5-year-old kid in the next. Your love for me expressed in quiet acts of service, in constant prayer, and most imminently in your presence with me, means more than you know. Thank you for readily giving me the space and time to pursue my interests even when they weren't the preferences you shared, and for this chance to embark on a faith journey together as a family.

And really, you are each channels of God's grace to me. For every new day I have had as a student in NUS, He has given new mercies and has never for a moment withdrawn His steadfast love. To be able to complete this project in spite of the unforeseen delays in between, I know it was not my effort, but His divine hand in it all. What can I say but thank YOU, Lord. To YOU be all the glory and praise.

"Remember my affliction and my wanderings,
the wormwood and the gall!
My soul continually remembers it
and is bowed down within me.
But this I call to mind,
and therefore I have hope:
The steadfast love of the LORD never ceases;
his mercies never come to an end;
they are new every morning;
great is your faithfulness.
'The Lord is my portion,' says my soul,
'therefore I will hope in him.' "

- Lamentations 3:19-24 (ESV)

Contents

Introduction

Understanding Aerosols

Within the Earth's gaseous atmosphere are aerosols – suspensions of small solid particles or liquid droplets which have a minimum atmospheric lifetime of 1 hour. Their physical dimensions range from a couple of nanometers to some tens of microns. They can be classified based on their origin – natural or anthropogenic. Natural aerosols include soot from combustion activity and sulfates derived from reactions of sulphur dioxide with atmospheric gases (Matthews, 2014). Anthropogenic aerosol sources include the burning of fossil fuels for transport and energy production, burning of biofuels, emissions from metallurgic and cement industries, and agricultural activity. Chemically, such atmospheric aerosols have inorganic and organic chemical components, as well as elemental carbon (Tomasi, Fuzzi, & Kokhanovsky, 2017).

Anthropogenic aerosols are usually confined to the lowest 2km of the atmosphere, and have a brief residence time of a few days, being eliminated dominantly by precipitation (Matthews, 2014). Aerosols generated by volcanic eruptions, however, can penetrate the next lowest atmospheric layer, the stratosphere, and circulate along with the global wind systems. One of the most notable examples is the 1991 eruption of Mount Pinatubo, an unprecedented event which led to a cooling of the lower atmosphere, reduction in solar heating and decrease in global temperatures by 0.6°C (Soden, Wetherald, & Stenchikov, 2002).

The above example fundamentally demonstrates that aerosols play a crucial role in the planetary radiative balance. Despite aerosol concentrations being markedly smaller than that of dominant air molecules, they are involved in a variety of processes within the atmosphere. These encompass their role as condensation nuclei for cloud formation and their potential to directly scatter or absorb insolation from the sun and terrestrial radiation leaving the Earth's

surface. Aerosols, then, constitute part of the planetary radiation budget, and have crucial influence in defining climate. Whether they contribute a net cooling or warming effect, however, is a complex matter dependent on factors of particle size and ground surface reflectance amongst others (Tomasi et al., 2017).

Anthropogenic aerosols constitute over 10% of the total aerosol mass loading, a fraction predicted to rise in the near future. Their effect on climate, however, is not well understood and requires further research through modelling and experiment (Tomasi et al., 2017). In this study, the main aerosols of interest are of anthropogenic origin; those emitted by urban fossil fuel burning and biomass burning. Oceanic dust, which has natural origin, is of lesser importance but is still present in Singapore owing to the close proximity to the sea (Salinas, Chew, & Liew, 2009). The following paragraphs are devoted to a more comprehensive understanding of each of these aerosol types.

Aerosols from Fossil Fuel Burning

Burning of fossil fuels produce black carbon (soot), organic carbon and sulphur dioxide which can subsequently be reacted to form sulphate aerosols. Globally, such combustion emits the most particulates into the atmosphere amongst all aerosol sources. According to forecasts, these emissions could double by the year 2040, with nations China and India being the main contributors (Tomasi et al., 2017). Even at present, a greater degree of coal and biomass burning takes place in Asia than in Europe or North America, which then contributes more absorbing soot and organic components to the Asian and Pacific atmospheres (Salinas et al., 2009). Studies performed by the National Aeronautics and Space Administration (NASA) suggest that sulphur-containing aerosols could have a cooling effect on the atmosphere (Gray, 2015).

On another note, the submicronic particles generated by burning of fossil fuels are also air pollutants and can have detrimental impacts on health and the

environment (Boucher, 2015). Growing industrialization and urbanization in Southeast Asia deem this a major concern (Chew et al., 2013). In view of the impacts on climate and health, aerosol-related research has grown over the years and continues to do so (Knippertz & Stuut, 2014).

Aerosols from Biomass Burning And Associated Meteorology

In this section, 'biomass' is understood to refer to biological material that could possibly be burnt, while fossil fuels that are formed on geological timescales are considered separately. The aerosols in question include both organic and black carbon, and can be materially observed in smoke plumes (Boucher, 2015).

Biomass burning in Southeast Asia is anthropogenic; naturally-occurring forest fires being rather atypical of the region. Intended for clearing forested areas and preparing the land for agricultural use, biomass burning has seen a substantial rise in the last 30 to 40 years. Intense dry seasons often lead to uncontainable spread of forest fires, thereby introducing smoke to neighbouring regions and triggering a decline in air quality (Chew et al., 2013).

Some meteorology is necessary to complete the picture. Singapore's close proximity to the equator (~1.2° North) defines her tropical climate of persistently high temperatures, rainfall and humidity. The change in wind directions between the monsoon seasons defines her local wind conditions (Velasco & Roth, 2012). As part of the Maritime Continent (MC), or tropical Southeast Asia, she experiences two monsoon seasons in a year: the Northeast monsoon from December to March, and the Southwest monsoon from June to September. These seasons are controlled by the movement of the Intertropical Convergence Zone (ITCZ) (Chew et al., 2013), a band of low-pressure extending in the east-west direction near the equator where the trade winds converge, migrating from around 30° North in June to 30° South in December and back (Oliver, 2005). The months from April

to May, and October to November are periods of transit from one monsoonal season to another (Chew et al., 2013).

During the Southwest Monsoon from June to September, that is, during the Northern hemisphere summer, dry conditions of reduced humidity and limited rainfall are ideal for biomass burning. In Sumatra, burning commences around July. The South-westerly flow brings the aerosols northward into Peninsular Malaysia and Singapore. The same low-latitude flows transport aerosols from biomass burning in Kalimantan into the South China Sea. Haze episodes in Singapore and Peninsular Malaysia are closely associated with these wind systems, and hence, see a similar seasonality (Chew et al., 2013). Examples of the most intense haze episodes experienced in Singapore include the periods: September-November 2006, October 2010, June 2013 and September-October 2015. A map of the Maritime Continent and associated wind flows, hotspot and hazy regions in September 2015 in Figure 1 below is reflective of what happens during a typical Southwest Monsoon. The hotspots shown are localized areas marked by hot and dry conditions, where biomass fires are most likely to occur.

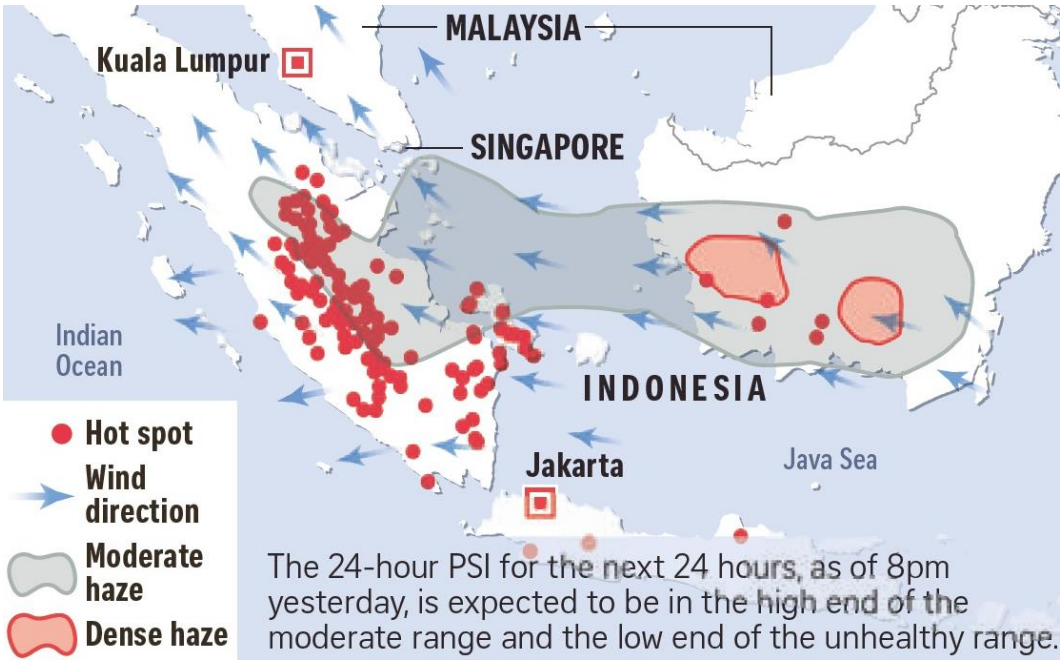

Figure 1: Map of Maritime Continent, with locations of hot spots, moderate haze, dense haze and wind directions denoted, for September 2015 (Meteorological Service Singapore, 2015)

During the Northeast Monsoon from December to March, dry conditions precede over Indochina while wet conditions dominate the MC. Beginning in February, biomass burning takes place in Indochina. Smoke particles are advected toward the MC through the North-easterly wind flow, where they are met with wet weather conditions. Aerosols arising from biomass burning expect to have an even shorter residence time in the local atmosphere. One should note still that while haze episodes occur mostly during the Southwest Monsoon, forest fires can ensue off-season and during the Northeast Monsoon as well, particularly when local weather experiences dryness and intense heat (Chew et al., 2013).

Aerosols from Oceanic Sources

The ocean generates sea-salt aerosols through a variety of physical processes. Such include the bursting of previously entrained air bubbles that had subsequently risen to the sea surface during whitecap formation, the efficacy of which depends on the wind speed. Oceanic aerosols are the second most abundant particulates by mass in the global troposphere, and in isolated oceanic regions, are the main radiative scattering species and the most important cloud condensation nuclei. This is realized only when the other aerosol types are present in relatively smaller abundances (Tomasi et al., 2017). Of the three aerosol sources discussed, the oceanic source is of the least importance to the discourse of Singapore's aerosol environment.

Previous Studies And Project Motivation

The Earth's energy budget is the balance of insolation from the sun and outgoing radiation from the earth. However, heat fluxes are altered by factors of land-use, cloud cover, albedo of surfaces and atmospheric composition, of which aerosols are an important constituent. Indirectly, they also affect heat flux through modification of cloud size. Quantitative and qualitative analysis of the aerosol radiative forcing is thus fundamental to climate studies. Though research on aerosols is increasing, their impact is still not comprehensively understood (Tomasi et al., 2017).

Singapore joined the Aerosol Robotic Network (AERONET) in October 2006, a sun photometer having been deployed at a site in the National University of Singapore (NUS) for the purpose of retrieving local aerosol properties and monitoring of the anthropogenic aerosol emissions from other countries in the MC as well. Aerosol-related research has been performed, with in-depth study of the physical and optical properties of a particularly significant climatic event or

over the span of 2 years at most. Others compared the aerosol optical properties spatially. Such studies are needful as the impacts aerosols have on climate depend heavily on their optical properties (Salinas et al., 2009), however little has been done on the temporal variations of these optical properties over an extended period of time.

This study is concerned with the temporal changes in the optical properties of aerosols, the period of interest spanning from November 2006, that is, when the Singapore AERONET site was started, to the present. These 10 years of AERONET data are sufficiently long to capture several intense haze episodes and slightly longer-term patterns in the aerosol optical properties in the absence of biomass burning events. These trends may then be used to understand and model the regional aerosol radiative forcing for the purpose of climate studies.

Project Objectives

The objectives of this project are twofold.

(1) To perform a statistical analysis of the aerosol characteristics (Aerosol Optical Depth and Angstrom Exponent number) from 2006 to 2015 retrieved from the Aerosol Robotic Network (AERONET).

(2) Across the same period of interest, to compute the aerosol radiative forcing using the LFLRT model (Fu & Liou, 1993) to evaluate and understand the impact of aerosols on the local climate.

Theory, Instrumentation and Methodology

Radiative Transfer Equation and the Plane-Parallel Atmosphere

The Radiative Transfer Equation (RTE) governs the propagation of radiation through a medium which can potentially scatter, absorb and emit. A schematic is used below to describe the elements involved in the RTE for a small segment of the propagating medium.

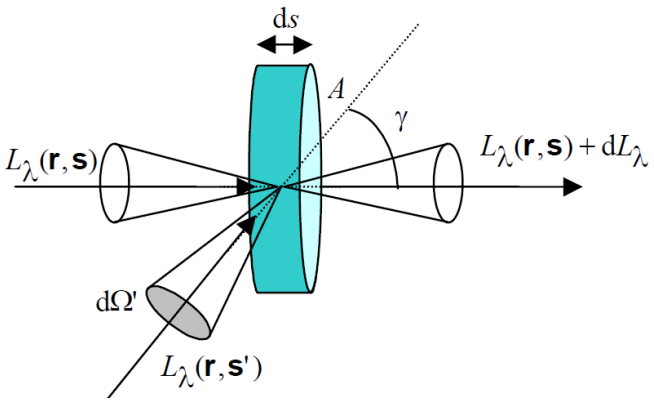

Figure 2: Component elements involved in derivation of RTE

The small segment placed at position $\boldsymbol{r} = (x, y, z)$, has dimensions reduced along one of its axes such that the infinitesimal thickness is $\mathrm{d}\boldsymbol{s}$, in a darker blue. The cross-sectional area A is denoted by the lighter blue shade. The direction normal to the area is taken to be $\boldsymbol{s}$, as parametrized by the zenith angle θ and the azimuthal angle ϕ. The beam along $\boldsymbol{s}$ has incident spectral radiance L_λ, which typically depends on both position $\boldsymbol{r}$ and direction $\boldsymbol{s}$. Radiance emerging from the transfer medium is denoted by $L_\lambda(\boldsymbol{r},\boldsymbol{s}) + dL_\lambda$, the radiance change term dL_λ owing to the processes that take place upon interaction of the direct beam with the medium. These include scattering and absorption of the direct beam, scattering

of incoming flux from other directions, and thermal emission. Monochromatic radiation is typically assumed.

Direct beam extinction is quantified in the Beer-Lambert-Bouguer law, which will be further discussed in the next section. The negative coefficient indicates a decreasing radiance:

$$dL_{\lambda,direct} = -L_\lambda(\boldsymbol{r},\boldsymbol{s})\,\beta_e(\boldsymbol{r},\lambda)\,ds \qquad (1)$$

The incident radiance can come from non-normal directions $\boldsymbol{s}'(\theta',\phi')$ as well. Upon scattering, they can increase the flux along the normal direction:

$$dL_{\lambda,scattered} = \frac{\omega(\lambda)\beta_e(\boldsymbol{r},\lambda)ds}{4\pi}\int_{all\ directions} L_\lambda(\boldsymbol{r},\boldsymbol{s}')\,P(\boldsymbol{s},\boldsymbol{s}',\boldsymbol{r},\lambda)\,d\Omega' \qquad (2)$$

Finally, the medium at temperature T will emit blackbody radiation in accordance to Planck's law. Along the normal direction $\boldsymbol{s}$, this increases the flux as modelled by the expression:

$$dL_{\lambda,thermal} = [1-\omega(\boldsymbol{r},\lambda)]\,\beta_e(\boldsymbol{r},\lambda)\,B_\lambda\big(T(\boldsymbol{r})\big)\,ds \qquad (3)$$

The sum of the changes in flux in Equations (1), (2), (3) yield the total radiance change of the beam along the $\boldsymbol{s}$ direction. The resulting expression can be written in the form:

$$\frac{1}{\beta_e(\boldsymbol{r},\lambda)}\frac{dL_\lambda(\boldsymbol{r},\boldsymbol{s})}{ds} = -L_\lambda(\boldsymbol{r},\boldsymbol{s}) + J_\lambda(\boldsymbol{r},\boldsymbol{s}) \qquad (4)$$

This is the RTE written in a general form. Appropriate boundary conditions would need to be prescribed in order to solve this equation for a given atmospheric profile.

Equation (4) includes a source function $J_\lambda(\boldsymbol{r},\boldsymbol{s})$ term. This source function accounts for all the scattering and emission in a given atmospheric profile, which are denoted by $J_{\lambda S}(\boldsymbol{r},\boldsymbol{s})$ and $J_{\lambda E}(\boldsymbol{r},\boldsymbol{s})$ respectively.

$$J_\lambda(\boldsymbol{r},\boldsymbol{s}) = J_{\lambda S}(\boldsymbol{r},\boldsymbol{s}) + J_{\lambda E}(\boldsymbol{r},\boldsymbol{s}) \qquad (5)$$

$$J_{\lambda S}(\boldsymbol{r},\boldsymbol{s}) = \frac{\omega(\boldsymbol{r},\lambda)}{4\pi}\int_{all\ directions} L_\lambda(\boldsymbol{r},\boldsymbol{s}')\,P(\boldsymbol{s},\boldsymbol{s}',\boldsymbol{r},\lambda)\,d\Omega' \qquad (6)$$

$$J_{\lambda E}(\boldsymbol{r},\boldsymbol{s}) = [1-\omega(\boldsymbol{r},\lambda)]\, B_{\lambda}\big(T(\boldsymbol{r})\big) \qquad (7)$$

The solution to the RTE is non-trivial, and is dependent on various atmospheric parameters. Nonetheless, some of the complexity can be eased by applying the Plane-Parallel Atmosphere approximation, wherein the surface of earth is treated as a flat plane. Above the surface, atmospheric composition is uniform in the horizontal direction and varies only along the vertical direction with increasing height above the ground.

In the schematic showing the components of the Plane-Parallel atmosphere (Figure 3), the xy −plane is taken to be the ground surface while the height above the ground varies along the z −axis. From this point, the position vector $\boldsymbol{r} = (x, y, z)$ can then be simplified to z. The RTE in Equation (4) is modified to become:

$$\frac{cos\theta}{\beta_e(z)}\frac{d}{dz}L_{\lambda}(z;\theta,\phi) = -L_{\lambda}(z;\theta,\phi) + J_{\lambda}(z;\theta,\phi) \qquad (8),$$

In a like manner, the corresponding Equations (5), (6) and (7) are simplified to:

$$J_{\lambda}(z;\theta,\phi) = J_{\lambda S}(z;\theta,\phi) + J_{\lambda E}(z;\theta,\phi) \qquad (9)$$

$$J_{\lambda S}(z;\theta,\phi) = \frac{\omega(z,\lambda)}{4\pi}\int_0^{2\pi}\int_0^{\pi} P(\theta,\phi,\theta',\phi';z,\lambda)\, L_{\lambda}(z;\theta',\phi')\, sin\theta'\, d\theta'\, d\phi' \qquad (10)$$

$$J_{\lambda E}(z;\theta,\phi) = [1-\omega(z,\lambda)]\, B_{\lambda}\big(T(z)\big) \qquad (11)$$

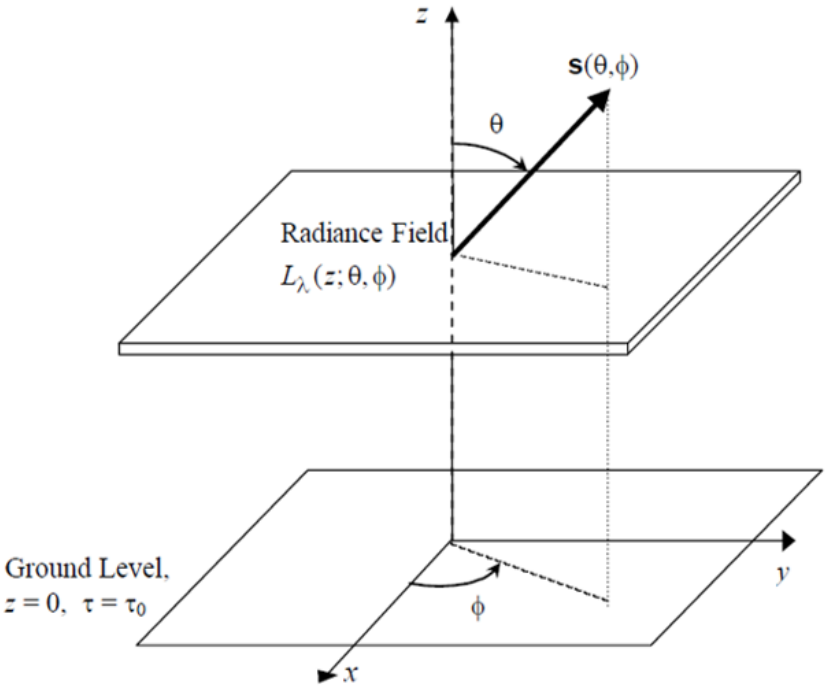

Figure 3: Components of the Plane-Parallel Atmosphere approximation

The parameter of optical thickness τ, which provides a measure of how opaque the propagating medium is to incident radiation, is used in place of altitude z. The optical thickness at a height z above the surface is defined by:

$$\tau(z,\lambda) = \int_z^\infty \beta_e(z',\lambda)\, dz' \qquad (12)$$

In reality, the upper limit of z' occurs at an altitude wherein the extinction coefficient of the air is nearly zero, and not at infinity. An analogous expression for the optical thickness at the ground surface may be written:

$$\tau_0 = \int_0^\infty \beta_e(z',\lambda)\, dz' \qquad (13)$$

As vertical height increases, the optical depth decreases. For a monochromatic radiation source, the derivative of the optical thickness is given by:

$$\frac{d\tau(z)}{dz} = -\beta_e(z) \qquad (14).$$

Here, we raise another variable $\mu = cos\theta$ for convenience. The directional dependence of μ on the zenith angle θ may be visualized in the following schematic:

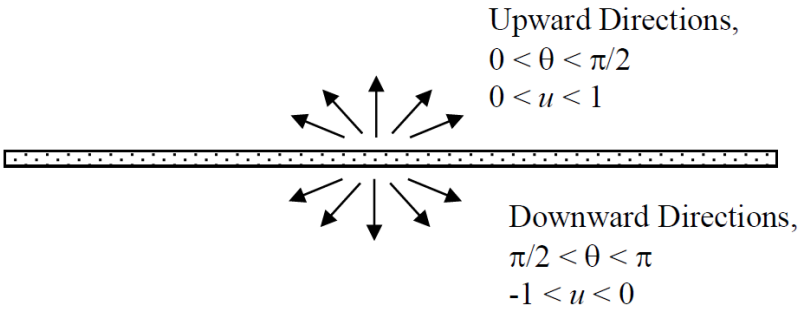

Figure 4: Upward and downward radiances

Finally, one arrives at a formulation of the RTE in terms of the new coordinates τ and μ for a Plane-Parallel atmosphere:

$$\mu \frac{d}{d\tau} L_\lambda(\tau;\mu,\phi) = L_\lambda(\tau;\mu,\phi) - J_\lambda(\tau;\mu,\phi) \qquad (15a),$$

or equivalently,

$$\frac{d}{d\tau} L_\lambda(\tau;\mu,\phi) - \frac{1}{\mu} L_\lambda(\tau;\mu,\phi) = -\frac{1}{\mu} J_\lambda(\tau;\mu,\phi) \qquad (15b).$$

with the total source function, and its component scattering and emission source functions respectively given:

$$J_\lambda(\tau;\mu,\phi) = J_{\lambda S}(\tau;\mu,\phi) + J_{\lambda E}(\tau;\mu,\phi) \qquad (16)$$

$$J_{\lambda S}(\tau;\mu,\phi) = \frac{\omega(\tau,\lambda)}{4\pi} \int_0^{2\pi} \int_0^{\pi} P(\mu,\phi,\mu',\phi';\tau,\lambda)\, L_\lambda(\tau;\theta\mu',\phi')\, d\mu'\, d\phi' \qquad (17)$$

$$J_{\lambda E}(\tau;\mu,\phi) = [1 - \omega(\tau,\lambda)]\, B_\lambda\big(T(\tau)\big) \qquad (18).$$

The integral in Equation (17) has yet to be solved because of the unknown radiance. An iterative method is one of the means to solve this. A preliminary approximation of the radiance is used to compute the source function, after which the source function is then substituted into the formal solution. Another radiance function is arrived at, which is used to find a new source function. This sequence is repeated until convergence happens.

For a scattering atmosphere, solar radiation passing through the atmosphere experiences both scattering and absorption. Thus, at any altitude, the radiance comprises 2 components. The first is due to the direct solar source, which is also taken as the incident radiance at the top of the atmosphere. This direct radiance experiences attenuation by the atmospheric layers. The second component is the diffuse radiation due to scattering within the atmosphere.

$$J_{\lambda S}(\tau;\mu,\phi) = \frac{\omega(\tau,\lambda)}{4\pi}\int_{0}^{2\pi}\int_{-1}^{1} P(\mu,\phi,\mu',\phi';\tau,\lambda)\, L_{\lambda,direct}(\tau;\theta\mu',\phi')\, d\mu'\, d\phi' + \frac{\omega(\tau,\lambda)}{4\pi}\int_{0}^{2\pi}\int_{-1}^{1} P(\mu,\phi,\mu',\phi';\tau,\lambda)\, L_{\lambda,diffuse}(\tau;\theta\mu',\phi')\, d\mu'\, d\phi' \quad (19)$$

Denoting the solar flux density at the top of the atmosphere ($\tau = 0$) as F, and the superscript s as the solar component, the direct radiance term is:

$$\frac{\omega(\tau,\lambda)}{4\pi}\int_{0}^{2\pi}\int_{-1}^{1} P(\mu,\phi,\mu',\phi';\tau,\lambda)\, L_{\lambda,direct}(\tau;\theta\mu',\phi')\, d\mu'\, d\phi' = \frac{\omega(\tau,\lambda)}{4\pi} F^{S} e^{-\tau/\mu^{s}}\, P(\mu,\phi,\mu^{s},\phi^{s};\tau,\lambda) \quad (20)$$

For the case of a scattering atmosphere illuminated by a solar source, numerical calculations are necessary for solving the RTE under particular input conditions (Goody & Yung, 1989). Suitable boundary conditions would need to be specified, so that upward and downward radiances can be computed for a given atmospheric profile. The Langley Fu and Liou Radiative Transfer model is used for this study. It solves Equation (15b) for a plane parallel atmosphere illuminated by a solar source at the top of the atmosphere, a lower boundary in the form of a uniform ground reflecting surface of fixed albedo, in the presence of aerosols and clouds. Fu and Liou (Fu & Liou, 1993) apply two analytical methods (2- and 4-stream method) to generate spectral irradiance fluxes at the top and bottom of the atmosphere. The fluxes are then computed by integrating L_λ over all stream directions as well as over shortwave and longwave spectral bands (Charlock et al., 2006).

Beer-Lambert-Bouguer Law

The Beer-Lambert-Bouguer law purports that the extinction of a beam of electromagnetic radiation as it is passed through an attenuating medium is given by the expression:

$$F(\lambda) = F_0(\lambda)e^{-\beta_e(\lambda)m(\theta)} \quad (21),$$

where F and F_0 give the wavelength-dependent solar irradiance, the former read at the instrument detector and the latter at the top of the atmosphere; β_e is the wavelength-dependent attenuation coefficient; m is the optical air mass, which is a function of θ, the solar zenith angle. The top-of-atmosphere solar irradiance $F_0(\lambda)$ can be determined from satellite measurements; the optical air mass m from solar angle measurements.

The slope of the linear fit of the logarithm of the solar irradiance detected by the photometer against the optical air mass returns the total atmospheric optical depth τ_t as expressed below:

$$\tau_t(\lambda) = \tau_a(\lambda) + \tau_R(\lambda) + \tau_g(\lambda) \quad (22).$$

Here, τ_a is the optical depth associated with atmospheric aerosols; τ_R is the optical depth relating to molecular scattering (Rayleigh scattering); τ_g is the optical depth due to molecular absorption. The sun photometer software provides the quantities τ_t and τ_R. For this study, the absorption term τ_g is treated as belonging to ozone gas alone, and can be calculated using known relationships.

The quantity of interest, the Aerosol Optical Depth τ_a, remains to be found, and depends on the specific center wavelength. The sun photometer takes measurements at 8 spectral bands, with center wavelengths at 340nm, 380nm, 440nm, 500nm, 675nm, 870nm, 1020nm and 1640nm. Strong spectral response occurs at wavelengths comparable to the aerosol particle size. Hence, 500nm is used as a reference in this study. With the Angstrom law, the expression for the aerosol optical depth becomes:

$$\tau_a(\lambda) = \tau_{a0}\lambda^{-\alpha} \quad (23).$$

τ_{a0} is the Aerosol Optical Depth at a reference wavelength at or near 1000nm; α is yet another aerosol optical parameter: the Angstrom Exponent number. Of the 8 spectral bands at which the photometer collects measurements, 2 are selected for the purpose of this study, and the logarithm of the wavelength λ plotted against the logarithm of τ_a. The gradient of the linear plot yields an equation from which the Angstrom Exponent number can be calculated:

$$\alpha = \frac{\ln[\tau_a(\lambda_2)] - \ln[\tau_a(\lambda_1)]}{\ln(\lambda_1) - \ln(\lambda_2)} \quad (24).$$

The above expression implies that the Angstrom Exponent number would differ based on the choice of λ_1 and λ_2. Percentage difference among the calculated values of α are minimized when a combination of the longest and shortest wavelengths is used. Further, instrumental noise is significant at short wavelengths while vapor absorption affects the longer wavelength channels. This motivates the choice of the wavelength range 440nm-870nm in computations of the Angstrom Exponent number for the purpose of this study (Salinas, Chew, & Liew, 2009b).

Aerosol Optical Depth And Angstrom Exponent

In this section, further attention is given to the 2 key aerosol parameters retrieved from the sun photometer and AERONET.

The Aerosol Optical Depth (AOD) measures the extinction of a direct beam of solar radiation due to aerosol absorption or scattering. The dimensionless quantity relates to the amount of aerosol vertically above the measuring photometer at unit cross-section, which inhibits incoming insolation from reaching the ground. Accordingly, the smaller the value of the AOD, the less polluted the atmosphere is by aerosols (Matthews, 2014).

The Angstrom Exponent number (AE) expresses the AOD as a function of the wavelength, and is frequently used as a qualitative indicator of particle size. The larger the exponent, the smaller the particle size (Matthews, 2014).

Optical properties are specific to the aerosol type. The table below documents the characteristic AOD and AE values for particular aerosols:

Aerosol Type	Aerosol Optical Depth	Angstrom Exponent
Urban Pollution	0.2 – 0.8	> 1.0
Biomass Burning Smoke	> 0.8	> 1.0
Oceanic	< 0.2	< 1.0
Dust	> 0.2	< 1.0

Table 1: Characteristic ranges of optical properties for different aerosol types (Knobelspiesse et al., 2004; Salinas, Chew, & Liew, 2009a; Eck et al., 2001)

One should recognize that while the above is a useful guideline for aerosol identification, it should not be applied as a deterministic measure. Consider, for instance, that intense urban pollution could yield AOD values greater than 0.8, which would lead to optical properties resembling the typical nature of biomass burning smoke. Further, the troposphere never contains only one aerosol type.

The measured optical properties for such a situation would then be a weighted average of the properties for each aerosol type present in the vertical column.

Sun Photometer And The Aerosol Robotic Network

A CIMEL Electronique CE-318A sun photometer is deployed on the rooftop of Block S17 at the National University of Singapore (NUS), around 30m above the ground. The automated instrument comprises an optical sensor head, a high precision robot and a control unit, is fully solar-powered, and can function reliably under diverse climatic conditions. The purpose of the photometer is mainly for quantification and characterization of the physical and optical properties of aerosols. Direct solar measurements are retrieved at 8 spectral bands at 30 second intervals. The altitudes at which particle species are located cannot be delineated, however, since the photometer views only the vertical column of atmosphere above it (CIMEL Advanced Monitoring, 2015). The instrument and its schematic are as shown in Figures 5 and 6 accordingly:

Figure 5: CIMEL Electronique CE-318 Sun Photometer
(CIMEL Climate Research Facility, 2015)

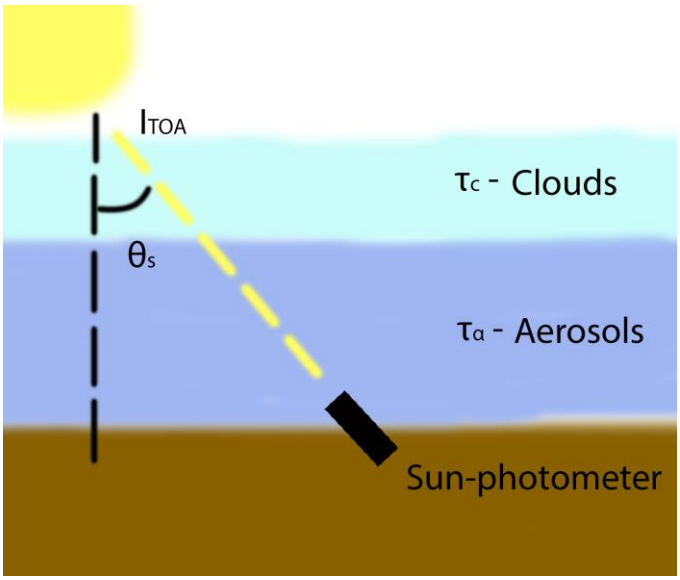

Figure 6: Simple schematic of the Sun-photometer

The instrument used for this study is labelled Number 22, and has been operational since October 2006 as part of the Aerosol Robotic Network (AERONET) partnership with the Centre of Remote Imaging, Sensing and Processing (CRISP) in NUS. More details about the AERONET worldwide network can be found at www.aeronet.nasa.gov.

AERONET data is classed into different levels according to the extent to which measurements have been cloud-screened. Level 1.0 raw data has not been passed through any form of cloud screening whatsoever. Implementing a cloud-screening algorithm yields Level 1.5 data. A final manual cloud-screening step gives Level 2.0 data (Smirnov et al., 2000).

In this study, data was retrieved from the Version 2.0 Direct Sun Algorithm. At Level 2.0, AOD measurements have passed through preliminary and final calibration, automatic cloud-screening and manual inspection, and are hence, quality-assured. The research interest in aerosols amongst all other atmospheric components demands data with minimal cloud-contamination, thereby motivating the choice of Level 2.0 data. For this study, daily averages of the AOD and AE for the period from November 2006 to August 2015 were retrieved for

analysis. A sample of AOD and AE data for Singapore in the year 2010 is presented in Figures 7 and 8 respectively.

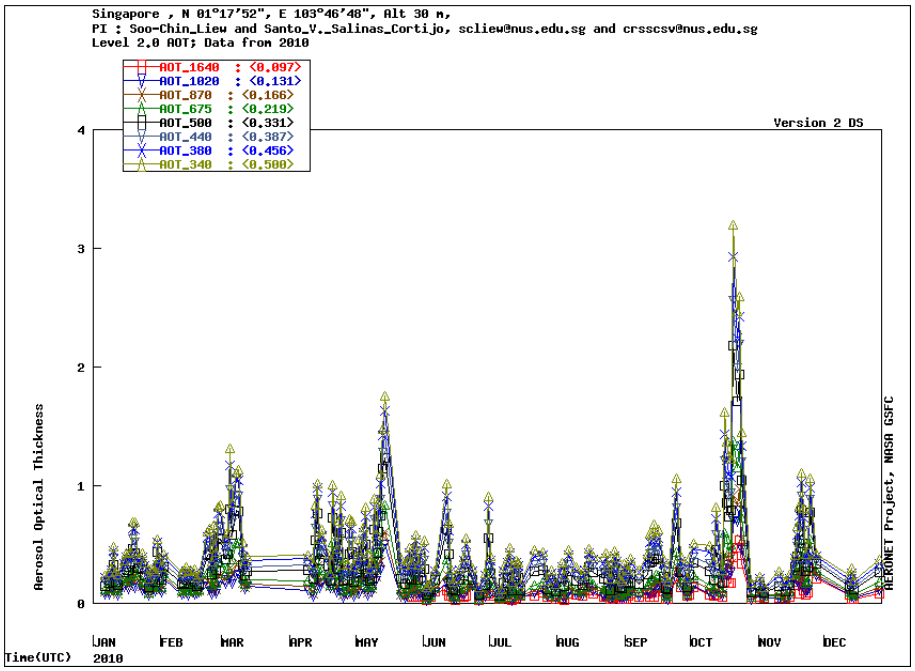

Figure 7: Sample AOD data for Singapore in 2010 retrieved from AERONET

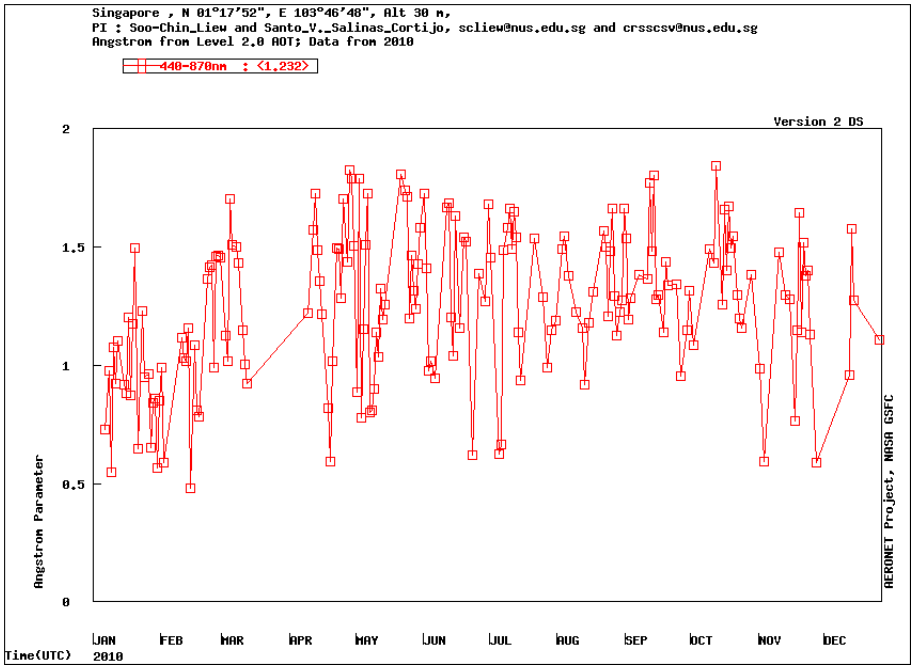

Figure 8: Sample AE data for Singapore in 2010 retrieved from AERONET

There is a west-bias to the AOD and AE data because of the location of the sun photometer. However, the same analysis performed on different spatial locations will likely produce similar results due to the small land area of Singapore. A previous study conducted using a hand-held sun photometer in the West and North of Singapore confirms this (Salinas, Chew, & Liew, 2009b).

Langley Fu & Liou Radiation Transfer Model

The original Fu and Liou Radiative Transfer code (1993) was developed based on this atmospheric model and had only 6 shortwave bands. It has since been modified by the NASA/Langley group studying heat fluxes from satellite data to include 29 such bands. Now referred to as the Langley Fu and Liou Radiative Transfer code (LFLRT), the model is part of the Clouds and the Earth's Radiant Energy System (CERES) (Charlock et al., 2006). In precise terms, the model uses a delta-four-stream method for radiative transfer in non-uniform atmospheres with gas, cloud, aerosol and Rayleigh molecule constituents (Liou, 2002), and can be effectively used for computing the radiative forcing for various cloud-aerosol atmospheric combinations, quick sensitivity studies, and tuning cases (Rose et al., 2005). Radiative fluxes at various altitudes are computed: at the top-of-atmosphere (TOA), within the atmosphere and at the ground surface. Such knowledge is critical since the disparity between the TOA and surface fluxes reveals whether the net radiative effect would be atmospheric heating or cooling (Charlock et al., 2006). In-flight calibration and comparison with other instrumentation allows for flux retrievals of less than 1% error (Smith et. al, 2011).

The model assumes a combination of clouds, gases and aerosols in the atmosphere. The radiative flux for the all-sky aerosol forcing is computed by subtracting the flux for an atmosphere composed of clouds and gases only from that of all-sky conditions. Clouds are absent from clear-sky computations. In like

manner, the clear-sky aerosol forcing is calculated by subtracting the forcing for a gas-only atmosphere from that of clear-sky conditions. The forcing calculations consider the following interactions between aerosols and radiation: longwave and shortwave scattering, longwave and shortwave absorption, and longwave emission. Fundamental input parameters include cloud area, cloud base height, optical depth, particle size, humidity, surface winds and ozone amongst others (Charlock et al., 2006).

NASA provides a daughter site for the CERES/ARM Validation Experiment (CAVE), on which the LFLRT code is available. Radiative fluxes may be computed either by downloading the source code, or by changing key atmospheric parameters directly on an interface on the site itself. The latter method was used for this particular study. An example of the interface and a sample of output data is presented in Figures 9 and 10.

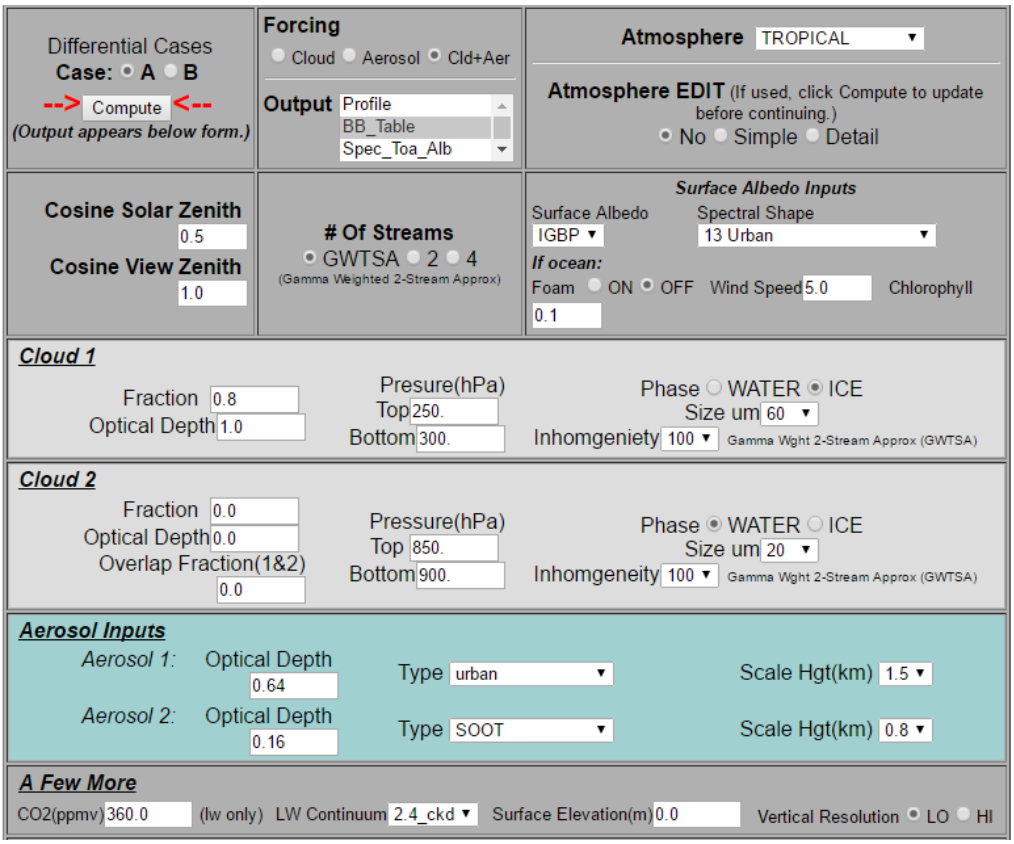

Figure 9: Online interface for the Langley Fu-Liou Radiative Transfer Model

CASE {A:Untuned} --> [PRISTINE] <-Vs-> [Cloud+Aerosol]						
Control : [PRISTINE]	SHORTWAVE Flux Wm-2					
Perturbed :[Cloud+Aerosol]	TOA			SURFACE		
Cloud& Aerosol	[PRISTINE]	[Cloud+Aerosol]	Forced	[PRISTINE]	[Cloud+Aerosol]	Forced
Up	125.4	189.7	64.3	88.6	56.3	-32.3
Down	682.5	682.5	0.0	476.0	278.0	-198.0
NET	557.1	492.8	-64.3	387.4	221.7	-165.7
ALBEDO	0.184	0.278	0.094	0.186	0.203	0.016
Direct				430.0	91.1	-338.9
Diffuse				46.0	186.9	140.9
Direct FuIceCor				430.0	48.8	-381.2
Diffuse FuIceCor				46.0	229.2	183.2
	LONGWAVE Flux Wm-2					
Up	287.5	231.2	-56.3	459.0	459.0	0.0
Down	0.0	0.0	0.0	398.1	404.6	6.5
NET	-287.5	-231.2	56.3	-60.8	-54.4	6.5

Figure 10: Sample output of the Langley Fu-Liou Radiative Transfer Model

Most of the input parameters are standardized using fixed atmospheric pre-sets. The aerosol inputs are varied according to the AOD data previously obtained from the AERONET site. The local atmosphere is treated as having cloud and aerosol components, and the flux computed with pristine conditions as the control atmosphere.

For each year of study, the mean AOD is computed for hazy and non-hazy periods respectively. The earlier meteorological discourse raised the Southwest monsoon season from June to September as the dominant period during which severe haze episodes take place in Singapore. Taking into account that the MC meteorological conditions experience some lag time in responding to the shifting ITCZ, the months of July, August, September and October are denoted the hazy months while the remaining times of the year are considered otherwise.

During non-hazy periods, the computed optical depth will be treated as that originating from urban pollution alone. During hazy periods, optical depth attributed to urban and soot aerosols requires some pre-treatment; the optical depth attributed to biomass due to soot during hazy seasons is approximated by computing 20% that of the total optical depth (Kirchstetter, 2004). The remaining 80% of the AOD figure is associated with urban pollution. Aerosol contribution by oceanic sources has been ignored since only 2 types of aerosol constituents are

permitted as inputs, and this source is of the least importance to Singapore's aerosol environment.

Using the outputs from the model, the net flux can be obtained by calculating the differences between the flux at the TOA and at the surface, and subsequently performing a qualitative analysis of the results. Aerosols, especially those of urban origin (mostly sulphates), are likely to reflect incoming radiation, hence generating a net cooling effect (Horning, Robinson, & Sterling, 2010). The same may be predicted of the computations; the hazy seasons are expected to have a stronger cooling effect than the non-hazy periods. However, aerosol from biomass burning (smoke) are absorbing particles and can heat the aerosol layer by absorbing incoming solar radiation. This generates some degree of uncertainty with regard to the net effect of aerosols once all of their contributions have been considered (Horning, et al., 2010).

Results And Discussion

Statistical Analysis of Aerosol Characteristics Over Time

A time series of the AOD and AE from November 2006 to August 2015 is shown in Figure 11. Dotted lines are used to demarcate the values 0.8 and 1.0 for the AOD and AE time series respectively. Both AOD and AE data is missing on particular days owing to the fact that the photometer cannot retrieve direct sun measurements on rainy days (CIMEL Advanced Monitoring, 2015).

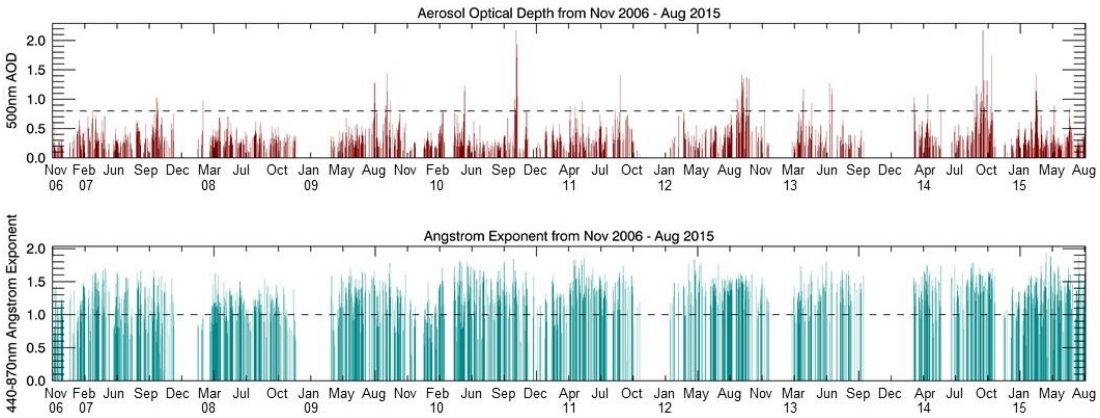

Figure 11: Time series of Aerosol Optical Depth and Angstrom Exponent number from November 2006 to August 2015

Previous sections of this report have stated the characteristic AOD and AE ranges for aerosols of different sources. As a recollection, urban pollution aerosols typically have AOD values ranging from 0.2 to 0.8 and AE values larger than 1.0. Aerosols originating from biomass burning have AOD values greater than 0.8 and AE values larger than 1.0.

Consequently, the AOD time series are helpful when discriminating between the relative dominance of aerosol type. The Figure 11 plot shows that AOD values

substantially larger than 0.8 do not occur at random, but during particular seasons – with an almost yearly occurrence from July to November, and the occasional isolated incident in March or April.

The seasonal patterns for these AOD values point to the presence of biomass burning smoke aerosols which are transported by regional wind systems from sources in Sumatra and Borneo to Singapore. Indeed, Southeast Asia is under the influence of the Southwest monsoon during the months from June to September, which bring about dry conditions over the region. When biomass burning commences in Sumatra around July, the South-westerly flow transports the smoke particles northward into Peninsular Malaysia and Singapore.

Peat burning is favourable during the South-west monsoon, but can occur during other times of the year as well. Studies on the aerosol environment in the MC in 2010 reported that though there was extensive cloud cover during the Northeast monsoon phase from January to March, hotspots were also constantly detected over the Sumatra and Peninsular Malaysia (Chew et al., 2013). Clearly, forest fires need not be confined only to periods with dry conditions. During off-season burning, smoke particles can be advected to Singapore via alternative transport mechanisms.

The AE time series shows values larger than 1.0 nearly all year round for all years under study. However, there is a noticeable oscillatory yearly behaviour which starts with low AE numbers at the beginning of each year, increases toward the middle, and decreases by the end of the 3rd quarter of the year. This behaviour is mostly induced by yearly transition from North-East to South-West monsoon and influenced by periods of dryness through the region.

There is a notable reduction of data points towards the end of each year, which is largely due to the beginning of the rainy season during late November and/or early December.

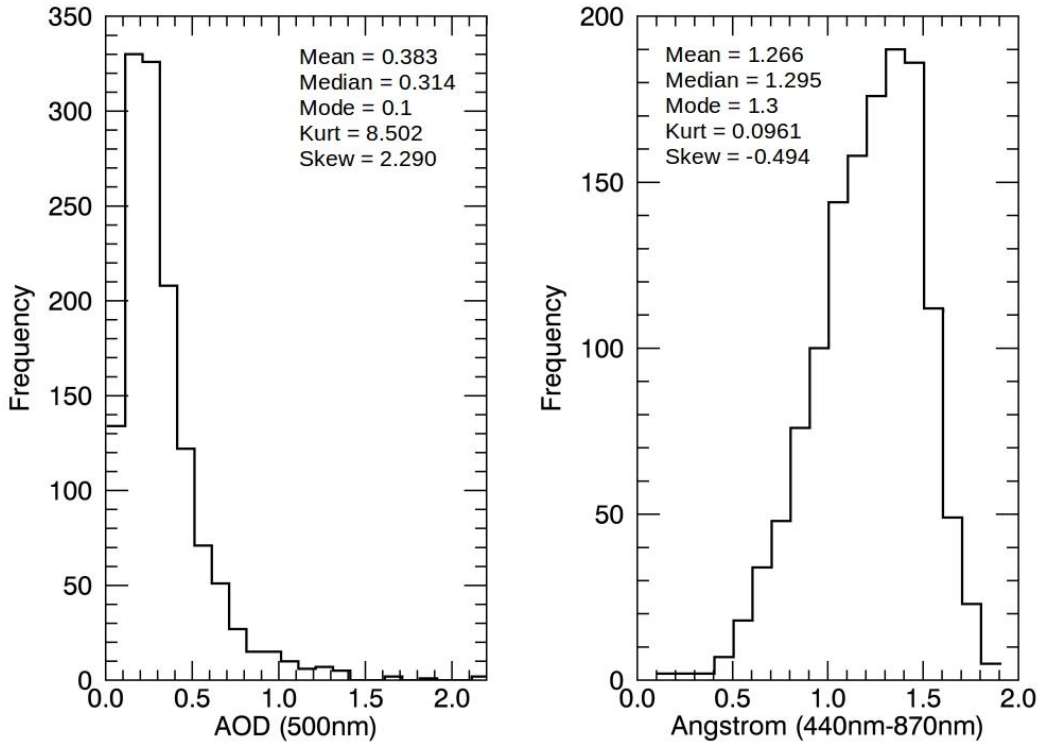

Figure 12(a): Histogram plots for the AOD and 12(b) AE from Nov 2006 to Aug 2015, with associated quantities of mean, median, mode, kurtosis and skewness value

From the frequency distribution in Figure 12(a), a distinct peak is observed at AOD values between 0.1 and 0.2, with the bulk of the distribution occurring at values smaller than 0.5. The relatively large and positive kurtosis value of 8.502 suggests a strong leptokurtic distribution with a sharp peak, while the positive skewness value of 2.290 denotes a longer tail toward the higher AOD values. However, AOD values greater than 1.0 show a low occurrence. The conclusion drawn from these, then, is that Singapore is predominantly under the influence of urban pollution aerosols during the year, with an additional biomass burning component during certain periods which are induced by periods of dry weather.

The AE histogram plot in Figure 12(b) peaks around 1.3, and its associated mean and median occur at 1.266 and 1.295 respectively, suggesting the values fall close to that of a normal distribution. The kurtosis of 0.0961 that is likely mesokurtic confirms this. The negative skewness of -0.494 points to a longer tail to the left

of the distribution maximum, with a small but measurable proportion of values falling below 1.0. These demonstrate that the local atmosphere is almost always populated with aerosols from either urban or biomass burning sources, but that maritime and dust aerosols could be present as well in small amounts.

To understand the temporal changes of the AOD (Figure 13) and AE (Figure 15), the histograms for each year from 2007 to 2015 were constructed and the distribution parameters indicated accordingly, the year 2006 excluded because the 2 months' worth of data would not have been representative of the entire year. The bracketed value of N on top of each histogram is the number of days for which measurements were taken for that year. Tables 2 and 3 shed light on the number of days for which the AOD and AE were larger than 0.8 and 1.0 respectively, and that as a fraction of the total number of days with available measurements.

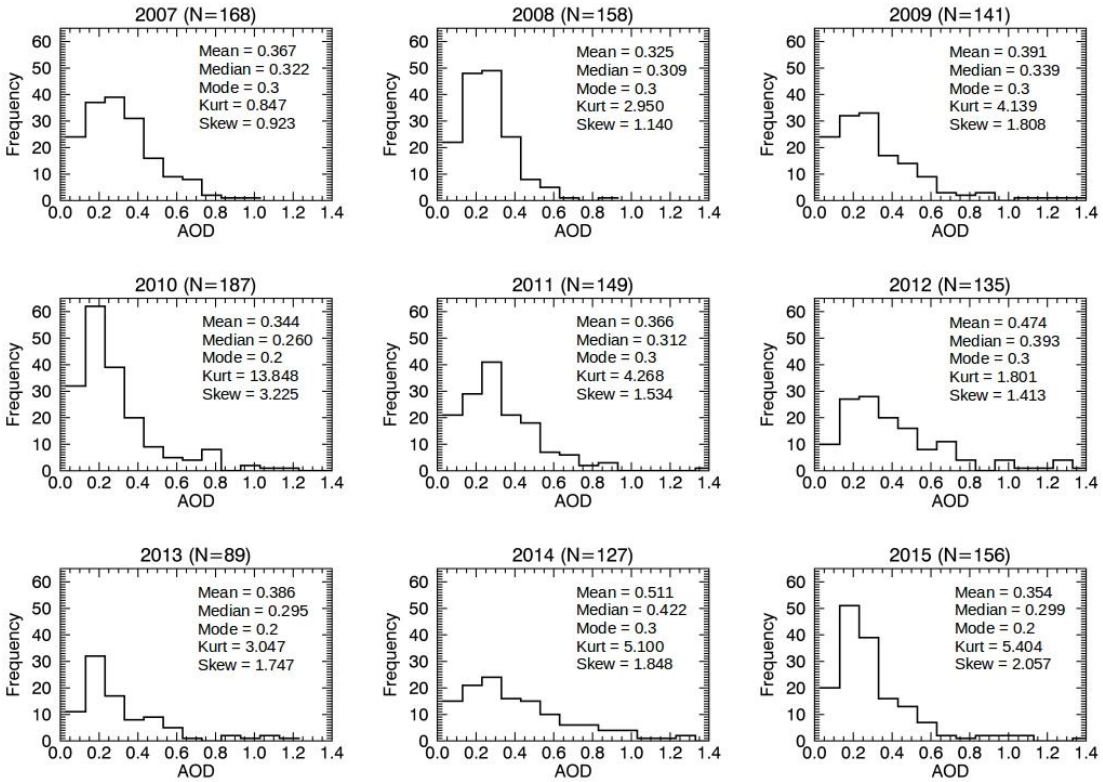

Figure 13: Yearly Histogram plots of AOD values with associated quantities of mean, median, mode, kurtosis and skewness

The yearly histogram plots alike report modes at around 0.2 to 0.3. Of specific interest are the skewness values, which increase steadily from 2007 to 2010, decrease from 2010 to 2012, and then increase again from 2012 to 2015. In spite of the actual number of days for which AOD > 0.8 being small, the broad conclusion drawn is that there is a growing spread toward higher AOD values. This points to a prolonged period of influence of biomass burning aerosols over Singapore, and should be carefully distinguished from the local source aerosols' residence time.

	2006	2007	2008	2009	2010	2011	2012	2013	2014	2015
No. Of Days	0	4	1	8	8	5	14	6	20	8
% of Total No. Of Days	0	2.38	0.63	5.67	4.28	3.36	10.37	6.74	15.75	5.13

Table 2: Number and percentage of days for which AOD > 0.8 from 2006 to 2015

Table 2 reports an interesting trend of the years with less severe haze episodes registering more days for which AOD > 0.8, as compared to the years which did experience intense haze conditions. Consider the years with relatively milder haze episodes in 2012 and 2014 which recorded 14 and 20 days respectively as compared to the years of notoriously haze conditions in 2010 and 2013 which had only 8 and 6 days accordingly. 21 June 2013 was the day the PSI index in Singapore hit its record high of 401 (Lee, 2015).

Such discrepancy arises intrinsically from how the aerosol parameters are computed. The AERONET Version 2.0, Level 1.5 data would already have been passed through a cloud-screening algorithm. Further manual cloud screening gives Level 2.0 data, which has been used in this study. When there is a high concentration of aerosols, which is expected of the years with intense haze episodes, aerosols can easily screened along with clouds, giving the false perception of an atmosphere less polluted than it is in reality. As a consequence,

there are fewer AOD > 0.8 days recorded, the error potentially being more pronounced in the years with more severe pollution.

A recently-released Version 3.0 of AERONET and its corresponding algorithm applied at Level 1.5 restores biomass burning smoke for high aerosol loading events (Giles et al., 2013). Ideally, the AOD data released under this version would produce a more reliable data set, if not for the fact that the final calibration has yet to be applied. The second-best option, Version 2.0, Level 2.0 data has been used in this research, but future studies could be greatly enhanced by use of the Version 3.0 Level 1.5 data when it has been quality-assured.

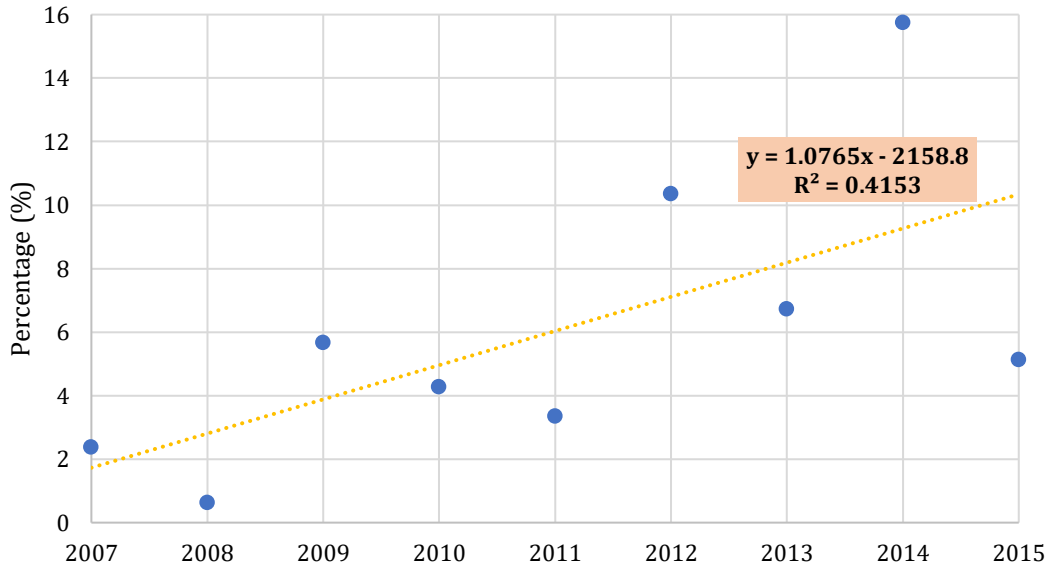

Figure 14: Data points indicating percentage of days for which AOD>0.8 as a function of the year (in blue), with linear fitting (in orange)

As a first estimate of the rate of increase in residence time, an additional graph plot using data from Table 2 was constructed. This is presented in Figure 14. The percentages plotted with reference to the year, with application of a linear fitting yielded a coefficient of determination of 0.415 and suggested a 1.07% increase in the proportion of days with AOD > 0.8 every year. This works out to 3.90 additional days under the influence of biomass burning aerosols per annum.

Visual inspection of the data points denotes alternating up-down fluctuations that become more marked with time amidst the general increasing trend. However, the years 2010, 2013 and 2015 should have slightly higher percentages than reported given they were marked by stronger haze episodes.

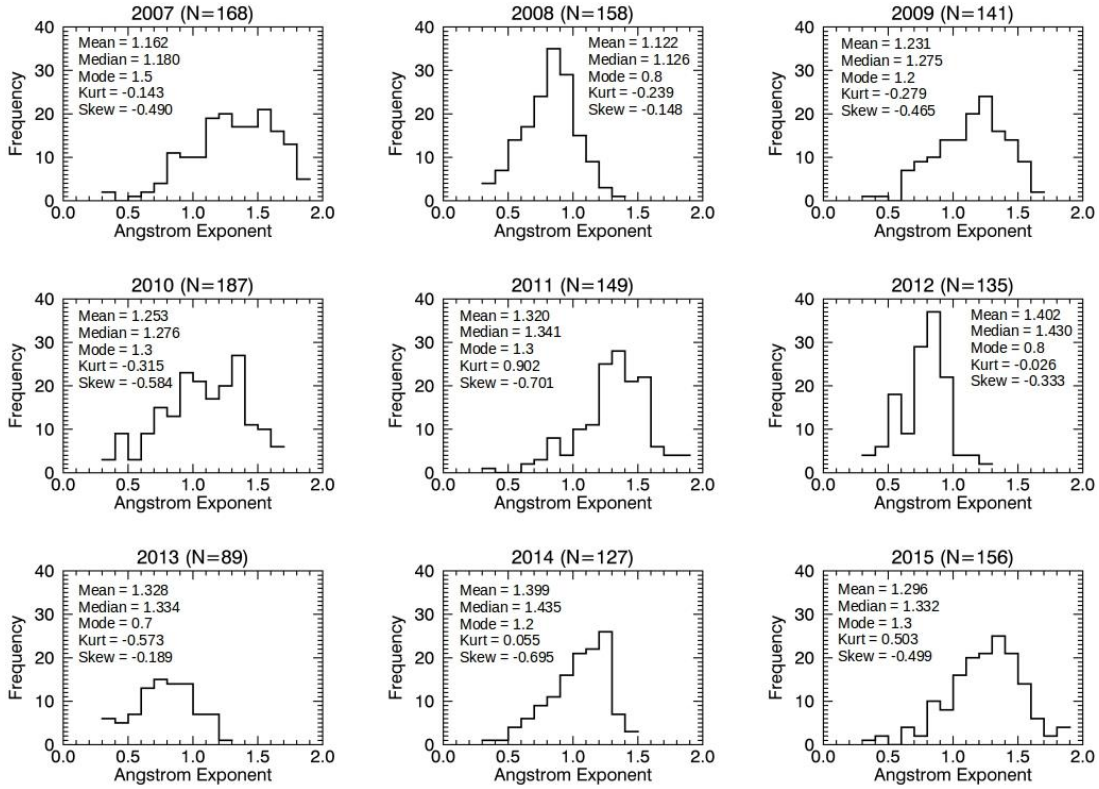

Figure 15: Yearly Histogram plots of AE values with associated quantities of mean, median, mode, kurtosis and skewness

Figure 15 gives the yearly AE histograms. With the exception of the years 2008, 2012 and 2013, the mode of the Angstrom histograms take on values greater than 1.0, reinforcing the previously established notion that the local atmosphere is, in general, composed of aerosols from either urban pollution sources or biomass burning.

	2006	2007	2008	2009	2010	2011	2012	2013	2014	2015
No. Of Days	12	116	116	111	144	132	131	81	117	132
% of Total No. Of Days	54.55	69.05	73.42	78.72	77.01	88.59	97.04	91.01	92.13	84.62

Table 3: Number and percentage of days for which AE > 1.0 from 2006 to 2015

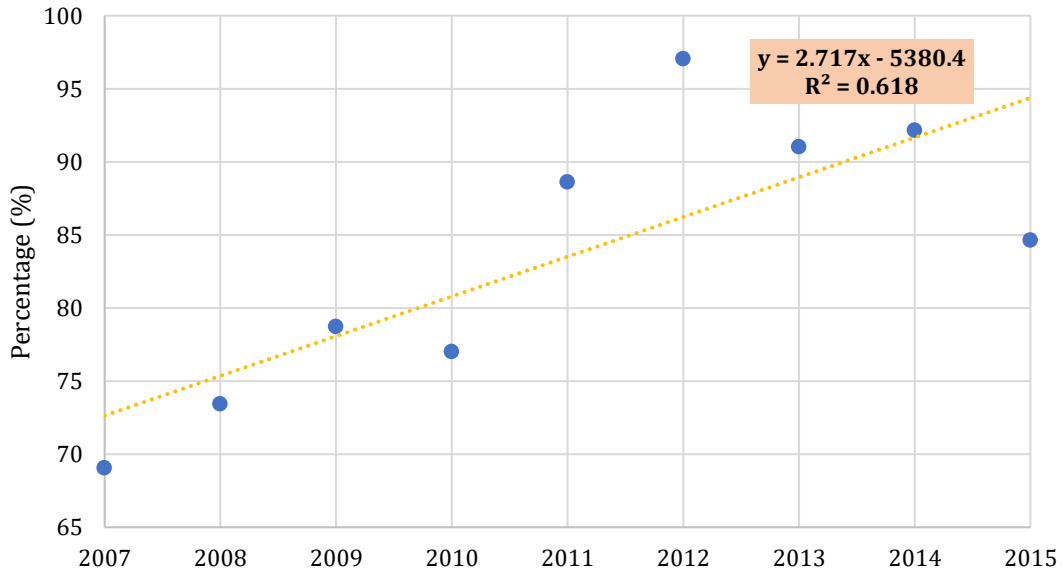

Figure 16: Data points indicating percentage of days with AE > 1.0 as a function of the year (in blue), and linear fitting (in orange)

Figure 16 shows the percentages in Table 3 as a function of the year. The linear fitting reports a coefficient of determination 0.618. The gradient indicates an increase of 2.717% per year, equivalent to an additional 9.86 days experiencing AE > 1.0 than the preceding year. This points to a prolonged influence of transboundary smoke and/or a growing intensity of local urban pollution over the years. Previously, the trendline of AOD > 0.8 in Figure 14 yielded an increase in 3.90 days yearly under the influence of transboundary smoke particulates. As an estimate, then, there is an increase in the 5.96 days recording AE > 1.0 because

of urban pollutant aerosols. The gradual increase in the AE over the years also indicates a reduction in the average particle size.

One intrinsic issue in this discussion is the lack of measurements on rainy days. Indicated on the yearly histograms, the number of days with AOD and AE data ranged from 89 to 187. For years with fewer measurements, namely 2013 in this case, the above discussion may not be sufficiently representative of the aerosol conditions for that year. Nevertheless, the rain on days without measured data would have caused extinction of the aerosols in the atmosphere.

Computation and Analysis of Radiative Heat Fluxes

The data presented in Table 4 provides a summary of the input variables used in radiative forcing modelling performed by the LFLRT code. The corresponding net fluxes at the TOA and surface in Table 5 are then added to give the net shortwave atmospheric flux. The different aerosol input values used did not alter the longwave fluxes appreciably; the net longwave flux at TOA occurs consistently around 56Wm^{-2} while the same quantity at the ground surface is approximately 5Wm^{-2}. These numerical values are used to compute the sum of the net longwave and shortwave fluxes in the atmosphere and are reported in Table 6. Negative fluxes indicate net cooling, while positive fluxes indicate net heating.

	Hazy Seasons (Jul-Oct)			Non-Hazy Seasons
Year	**Average Total AOD**	**Biomass Burning AOD**	**Urban Pollution AOD**	**Average Total AOD**
2006	-	-	-	0.24824
2007	0.40268	0.080536	0.322144	0.34369
2008	0.31311	0.062622	0.250488	0.33349
2009	0.50121	0.100242	0.400968	0.30184
2010	0.35651	0.071302	0.285208	0.33508
2011	0.43411	0.086822	0.347288	0.32823
2012	0.60172	0.120344	0.481376	0.35099
2013	0.30413	0.060826	0.243304	0.42702
2014	0.57293	0.114586	0.458344	0.44216
2015	1.41839	0.283678	1.134712	0.37841
2016	0.27390	0.054780	0.21912	0.33631

Table 4: AOD inputs used for radiative flux calculations

Aerosol parameters only up to August 2015 had been available on the AERONET site previously. During the course of this project, in March 2017, data for the remaining months of 2015 and the entire 2016 were released. Owing to time constraints, these measurements were excluded from the previous quantitative

and qualitative analysis of aerosol particle characteristics, but have been included in the present study on computation and analysis of heat fluxes.

	Hazy Seasons (Jul-Oct)			Non-Hazy Seasons		
Year	Net Flux at TOA	Net Flux at Surface	Combined Flux	Net Flux at TOA	Net Flux at Surface	Combined Flux
2006	-	-	-	-69.1	-76.0	-145.1
2007	-62.1	-116.3	-178.4	-72.9	-84.8	-157.7
2008	-61.4	-103.3	-164.7	-72.5	-83.9	-156.4
2009	-62.8	-129.8	-192.6	-71.3	-81.0	-152.3
2010	-61.7	-109.7	-171.4	-72.6	-84.0	-156.6
2011	-62.4	-120.7	-183.1	-72.3	-83.4	-155.7
2012	-63.4	-142.6	-206.0	-73.2	-85.5	-158.7
2013	-61.3	-102.0	-163.3	-76.0	-92.1	-168.1
2014	-63.2	-139.0	-202.2	-76.5	-93.4	-169.9
2015	-66.1	-222.1	-288.2	-74.2	-87.9	-162.1
2016	-61.0	-97.4	-158.4	-72.6	-84.2	-156.8

Table 5: Net shortwave radiative fluxes at TOA, ground surface and combined

	Hazy Seasons (Jul-Oct)	Non-Hazy Seasons
Year	Total Net Flux	Total Net Flux
2006	-	-84.1
2007	-117.4	-96.7
2008	-103.7	-95.4
2009	-131.6	-91.3
2010	-110.4	-95.6
2011	-122.1	-94.7
2012	-145.0	-97.7
2013	-102.3	-107.1
2014	-141.2	-108.9
2015	-227.2	-101.1
2016	-97.4	-95.8

Table 6: Net heat flux for sum of longwave and shortwave contributions

The sum of the longwave and shortwave contributions yield negative values for all the years and seasons of interest, in line with the understanding that aerosols tend to reflect radiation and generate a net cooling effect on the atmosphere

(Horning, Robinson, & Sterling, 2010). With the exception of 2006, during which data retrieval had yet been made available for the months of July to October, and 2013, the net heat flux for the hazy seasons is consistently larger than that for the non-hazy seasons. This confirms the earlier discussion; seasons with biomass burning activity tend to have larger AOD values. Since the AOD is a measure of the amount of aerosol vertically above the measuring photometer, one would naturally anticipate stronger cooling for the hazy seasons. In spite of the smoke aerosols contributing a rather small 20% fraction of the total aerosol optical depth during the hazy seasons, its impact on the radiative flux is clearly measurable.

The earlier discussion on the years with less severe haze conditions appearing to have fewer AOD > 0.8 days recorded is carried into this section on radiative fluxes. The years 2008, 2012 and 2014 had significantly more negative forcing values despite experiencing moderate haze during these years. This relates intrinsically to the AERONET cloud-screening processes which mistakenly screen thick aerosol layers as clouds. The removal of these particulates may possibly have led to such significant decrease in AOD that for 2013, the non-hazy season computed stronger reflectance than its hazy counterpart.

The remaining months of 2013 following the biomass burning season also did not measure any aerosol properties by the sun photometer. This means the non-hazy season comprised only 6-months-worth of data from January to June only, during which there were several AOD > 0.8 instances, potentially leading to an upward bias of the average AOD computed for regular conditions.

The year 2015 stands out, recording a yearly AOD value of 1.418, which is a disturbingly large value referenced against the typical average of around 0.3 to 0.5. The effects on insolation are equally distressing; the net flux during the months July to October is $-227.2\mathrm{Wm}^{-2}$, a figure almost twice the magnitude of any of the other years, and likely entailing a cooling effect twice as effective. One should note the break in the vertical axis from $-150\mathrm{Wm}^{-2}$ to $-230\mathrm{Wm}^{-2}$ in Figure 17 below. These, however, should not come as a surprise, given the 2015 transboundary haze crisis in the MC was remarked one of the worst on record. A

report by NASA-based scientist Dr Robert Field cited "(c)onditions in Singapore and south-eastern Sumatra... tracking close to 1997" (Chan, 2015). The prolonged influence of the haze over Singapore that year has since been attributed to the moderate El Nino in Indonesia which strengthened and extended the dry conditions of the Southwest monsoon (National Environment Agency, 2015a). The eventual subsiding of the air pollution in Singapore was atttributed to the change in wind conditions and not the subsiding of hotspots in Sumatra (National Environment Agency, 2015b). Further, one must recognize that these extreme values resulted even after the cloud-screening algorithm and manual processing had removed some amount of aerosol. In reality, then, the average AOD for the hazy season of 2015 should be higher, the net radiative forcing more negative, and the net atmospheric effect more strongly cooling.

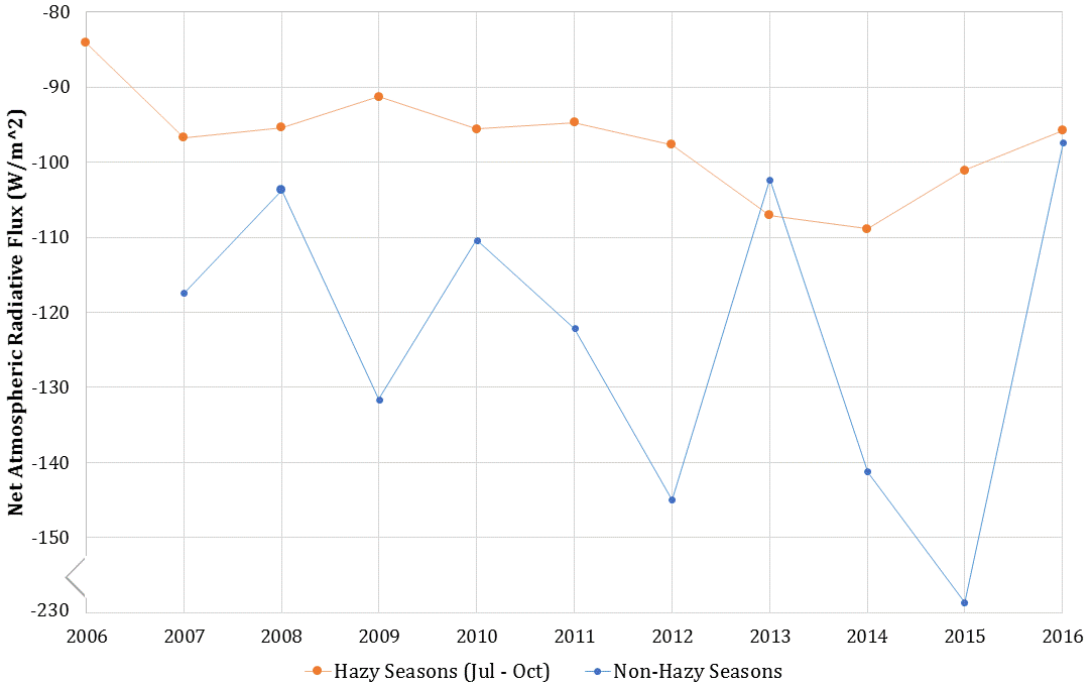

Figure 17: Time series of net atmospheric radiative forcing for both hazy and non-hazy seasons

With regard to the effects on local climate, however, the impacts of these smoke aerosols are not as critical compared to that of urban pollution aerosols. While

the radiative forcing can be measurably increased during the Southwest monsoon months, biomass burning aerosols will be promptly removed by wet scavenging and dry deposition processes (Matthews, 2014), deeming their climatic influence on the local atmosphere rather short-lived. On the other hand, the contribution from urban pollutants is present all year-round. As much as these aerosols can be quickly removed by precipitation, they will be quickly and continually emitted again by local urban sources.

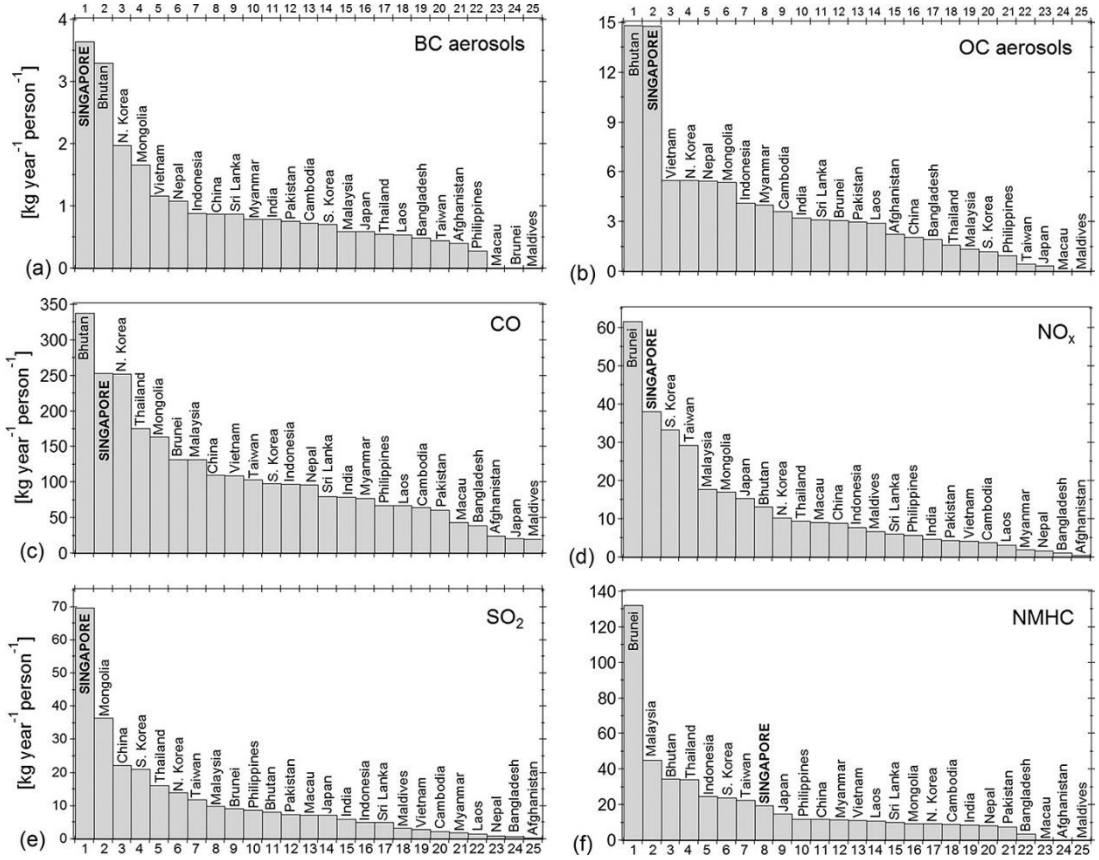

Figure 18: Per-capita anthropogenic emissions of (a) black carbon aerosols, (b) organic carbon aerosols, (c) CO, (d) NOx, (e) SO2, and (f) NMHC from 25 Asian countries (Ohara et al., 2007)

Very broadly, one observes a decreasing net radiative forcing (or increasing net cooling effect) from 2006 to 2016. Practically, from these one may conclude that urban pollution is growing gradually in intensity or concentration. Some

increases in forcing occur in between – from 2007 to 2009, from 2010 to 2011, and from 2014 to 2016, which sees one of greater magnitude. These fluctuations are significantly smaller in magnitude compared to that of the hazy seasons, and could be the culmination of growing effort to minimize pollutant emissions against the backdrop of growing industry. Singapore's air quality indicators comply with international standards by many measures, but the per-capita anthropogenic contributions for various pollutants are by no means low (Velasco & Roth, 2012), as Figure 18 shows.

Throughout the computation and analysis of the radiative forcing due to aerosols, the particulates have been treated exclusively as aerosols. In other words, only the direct impacts of aerosols on climatology have been computed. Some of the more notable indirect impacts – aerosols acting as nuclei for condensation leading up to cloud formation, modification of cloud size, and the consequent effect on rainfall – remain unknown from these calculations alone. In the tropics, clouds have been found to have "near cancellation" of radiative longwave warming and shortwave cooling. However, changes in cloud cover can upset this balance easily, and large masses of aerosols have potential to do so (Schmidt, 2001).

Owing to the nature of the radiative transfer model used, only 2 aerosol types are allowed as inputs, inevitably overlooking the contribution from oceanic sources. While oceanic aerosols could have been included as the 2nd input aerosol during non-hazy seasons, the fluxes from these periods would no longer serve as an effective basis of comparison for the forcings computed for the hazy periods had this been performed. This would have reduced the accuracy of our calculations somewhat and hence the climatic effects of biomass burning particulates.

Further, the exact ratio of the urban to biomass burning aerosols is not known. The value of 20% transboundary smoke particulates to 80% urban pollution aerosols during the hazy seasons is based on previous research. Strong South-westerly winds coupled with intense burning from the source regions are expected to bring in greater concentrations of biomass burning aerosols, which could raise the percentage to over 20%. In the converse situation, or when there

are mechanisms which remove some of the particulates, the 20% of transboundary smoke aerosols could be an over-estimate.

Another issue arising from the processing of AOD for calculation of the radiative forcing is that haze has been taken to occur exclusively during the months July to October. As was mentioned in the statistical analysis of aerosol properties, transboundary smoke can be advected to Singapore during other periods as well. A small fraction of the average AOD computed for non-hazy months is thus caused by biomass burning aerosols. However, the relative proportion during these seasons is not known. This leads to a calculated net radiative forcing of smaller magnitude than the reality is.

Likewise, biomass smoke is not a constant presence throughout the hazy seasons; a measurable number of days experience conditions typical of the non-hazy periods; aerosols from urban pollution sources dominating. This generates an upper bias to the radiative forcing computed for hazy periods. Putting these two contributions together, the disparity in the net atmospheric radiative forcing for hazy and non-hazy periods should be slightly smaller than what has been presented earlier in Figure 17.

Having put forth this discussion relating to the radiative forcing and climatic impact of aerosols, one must recall that aerosols are merely a single component of the atmospheric radiation and heat balance. That is not to discount the effect of aerosols, but to highlight that they are part of a system and are closely integrated with other atmospheric components. Since the atmosphere must respond to the net impacts of all possible radiative forcings, a detailed understanding of local climate cannot be complete until all, or at least the major components have been studied.

Finally, the discussion in light of these remains confined to impacts on the local climate. While these measurements cannot provide a comprehensive picture of regional impacts, other studies have shown that the organic compounds generated by the burning of rainforests in Southeast Asia, when interacted with anthropogenic pollutants, can trigger disturbances in the troposphere at a

regional scale, and possibly even a global scale (Hewitt et al., 2010). These conditions are met in Singapore during the seasons with transboundary smoke. However, potential interactions between aerosol types of different chemical species, and their consequent climatic effects are not explored in this study.

Conclusion

Summary

As part of this project, aerosol optical characteristics – the AOD and AE – from November 2006 to December 2016 were retrieved from the AERONET site. The time series and histograms for the respective physical and optical properties of aerosol particles were retrieved and analysed quantitatively and qualitatively.

From the processing of the aerosol properties, it was found that biomass burning aerosols occur at specific times of the year corresponding to the Southwest Monsoon from June to September. There are a few instances of transboundary smoke presence at other times of the year due to other transport mechanisms. Nevertheless, Singapore is under the persistent influence of urban pollution aerosols throughout the year, with a small percentage of maritime and dust aerosols as well. The temporal analysis points to a growing time of influence of both smoke and urban pollution particulates, and a reduction in aerosol particle size over the years. The severity of such seasons cannot be determined from these measurements alone.

The AOD data was also used to compute the aerosol radiative forcing using the LFLRT model, in a bid to understand the impacts of aerosols on local climate. All of the inputs yielded net cooling effects over a prescribed atmospheric profile. The hazy seasons in a year almost consistently recorded a higher radiative forcing than its non-hazy season counterpart, indicating a stronger net reflectance and cooling.

Nonetheless, some of the other impacts of aerosols are not fully captured in the calculations and analyses presented in this study. The atmosphere, even over the small region of Singapore, is an intricate system combining the effects of many component parts in which several feedback mechanisms take place, particularly between aerosols and clouds.

Further Work

The existing study can be furthered in several ways. For one, more detailed analysis can be performed for particularly significant climatic events using data retrieved from the Micropulse Lidar Network (MPLNET). The lidar instrument transmits a pulse of laser energy vertically upward into the atmosphere. Backscattered signals are then used to profile the altitude at which clouds and aerosols are present. The aerosol height can be included in computations using the LFLRT model for a more accurate computation of the net aerosol radiative forcing.

Qualitative analysis can also be performed on other aerosol optical properties available for retrieval from the AERONET site. Such include the particle size distribution, the scattering phase function and the single-scattering albedo amongst many others. It could be instructive to plot a time series of parameters such as the Multivariate ENSO Index (MEI), the daily MODIS hotspots over the Maritime Continent, the PM_{10} and $PM_{2.5}$ concentrations as well, especially during the Southwest monsoon months.

Finally, since one of the research intents is to understand aerosol radiative forcings for the region, a spatial analysis would prove useful. Aerosol properties in Kuching and Penang, both of which are in Malaysia, can be obtained from the AERONET site and compared against the aerosol optical characteristics of Singapore. Such study would be highly instructive since all three locations are under the influence of the same regional wind systems, and have the same biomass particulate sources.

References

Bowman, K. P. (2006). *An Introduction to Programming with IDL*. Amsterdam; Boston: Elsevier Academic Press.

Boucher, O. (2015). *Atmospheric Aerosols: Properties and Climate Effects.* Dordrecht: Springer Netherlands.

Chan, F. (2015, October 3). Haze crisis set to be 'one of the worst on record'. *The Straits Times*.

Charlock, T. P., Rose, F. G., Rutan, D. A., Jin, Z., & Kato S. (2006). Proceedings 12th Conf. on Atmos. Radiation: *The Global Surface and Atmospheric Radiation Budget: An Assessment of Accuracy With 5 Years of Calculations and Observations*. Madison: WI.

Chew, B.N., Campbell, J. R., Salinas, S. V., Chew, W. C., Reid, J. S., Welton, E. J., Holben, B. N., Liew, S. C. (2013). Aerosol particle vertical distributions and optical properties over Singapore, *Atmospheric Environment, 79,* 599-613. doi: http://dx.doi.org.libproxy1.nus.edu.sg/10.1016/j.atmosenv.2013.06.026

CIMEL Advanced Monitoring. (2015). *Multiband Photometer CE318-N User's Manual*.

Eck, T. F., Holben, B. N., Dubovik, O., Smirnov, A., Slutsker, I., Lobert, J. M., & Ramanathan, V. (2001). Column - integrated aerosol optical properties over the maldives during the northeast monsoon for 1998 – 2000. *Journal of Geophysical Research: Atmospheres, 106*(D22), 28555-28566. doi:10.1029/2001JD000786

Fu, Q., Liou, K. N.(1993). Parameterization of the radiative properties of cirrus clouds. *Journal of Atmospheric Science. 50* (13), 2008–2025. doi:10.1175/1520-0469(1993)050<2008:POTRPO>2.0.CO;2.

Giles, D., Holben, B., Smirnov, A., Eck, T., Slutsker, I., Sorokin, M., Schafer, J., Sinyuk, A. (2013). Yoram Kaufman Memorial Symposium presentation: *Evaluation of AERONET AOD Measurements in the Version 3 Database*.

Goody, R. M., & Yung, Y. L. (1989*). Atmospheric radiation: Theoretical basis* (2nd ed.). New York: Oxford University Press.

Gray, R. (2015, December 21). Forget global warming, pollution can actually COOL the planet: Aerosols from burning fossil fuels may protect some regions from the effects of climate change. *Mail Online*. Retrieved from: http://www.dailymail.co.uk/sciencetech/article-3368886/NASA-study-Examination-Earth-s-recent-history-key-predicting-global-temperatures.html

Hewitt, C. N., Lee, J. D., MacKenzie, A. R., Barkley, M. P., Carslaw, N., Carver, G. D., . . . Yin, X. (2010). Overview: Oxidant and particle photochemical processes above a south-east asian tropical rainforest (the OP3 project): Introduction, rationale, location characteristics and tools. *Atmospheric Chemistry and Physics, 10*(1), 169-199. doi:10.5194/acp-10-169-2010

Horning, N., Robinson J. A., Sterling E. J. (2010). *Remote sensing for ecology and conservation: A handbook of techniques.* Oxford: Oxford University Press.

Kirchstetter, T. W., Novakov, T., & Hobbs, P. V. (2004). Evidence that the spectral dependence of light absorption by aerosols is affected by organic carbon. *Journal of Geophysical Research - Atmospheres, 109*(D21), D21208-n/a. doi:10.1029/2004JD004999

Knippertz, P., & Stuut, J. W. (2014). *Mineral dust: A key player in the earth system*. Dordrecht: Springer.

Knobelspiesse, K. D., Pietras, C., Fargion, G. S., Wang, M., Frouin, R., Miller, M. A., . . . Balch, W. M. (2004). Maritime aerosol optical thickness measured by handheld sun photometers. *Remote Sensing of Environment, 93*(1), 87-106. doi:10.1016/j.rse.2004.06.018

Koh, X. H. (2015, November 17). Haze Subsidy Scheme to cease on Monday. *The Straits Times*.

Lee, M. K. (2015, October 2). Haze in Singapore: A problem dating back 40 years. *The Straits Times.*

Liew, S. C. (2014). *Radiative Transfer Equation*. Personal Collection of Liew Soo Chin, National University of Singapore, Singapore

Liou, K. N., (2002). *An Introduction to Atmospheric Radiation* (2nd Ed.). Amsterdam; Boston;: Academic Press.

Matthews, J. A., (2014). *Encyclopedia of Environmental Change*. United Kingdom: SAGE Publication, Ltd. doi:http://dx.doi.org.libproxy1.nus.edu.sg/10.4135/9781446247501

National Environment Agency. (2015, September 28). Haze situation update – NEA sends preventive measures notice to sixth company. *Advisories*. Retrieved from: http://www.nea.gov.sg/corporate-functions/newsroom/advisories

National Environment Agency. (2015, October 12). Haze situation update. *Advisories*. Retrieved from: http://www.nea.gov.sg/corporate-functions/newsroom/advisories

Ohara, T., Akimoto, H., Kurokawa, J., Horii, N., Yamaji, K., Yan, X., & Hayasaka, T. (2007). An asian emission inventory of anthropogenic emission sources for the period 1980-2020. *Atmospheric Chemistry and Physics, 7*(16), 4419-4444. doi:10.5194/acp-7-4419-2007

Oliver, J. E. (2005). *The encyclopedia of world climatology*. Dordrecht: Springer. doi:10.1007/1-4020-3266-8

Rose, F., Fu, Q., Charlock, T., Karo, S., Kratz, D., Rutan, D., Jin, Z. (2005). *CERES SARB On-line Fu-Liou Radiative Transfer Code Differential 200503 Version* [Powerpoint Slides]. Retrieved from: https://ceres.larc.nasa.gov/documents/STM/2005-05/rose-sarb.pdf

Rose, F., Fu, Q., Charlock, T., Karo, S., Kratz, D., Rutan, D., Jin, Z. (2007). *CERES PROTO-Edition Radiative Transfer: Model Tests and Radiative Closure Over Surface Valadation Sites*. Retrieved from: https://ams.confex.com/ams/pdfpapers/112358.pdf.

Salinas, S.V., Chew, B.N., & Liew, S.C. (2009). Retrievals of aerosol optical depth and angstrom exponent from ground-based Sun-photometer data of Singapore. *Applied Optics, 48* (8), 1473–1484. doi:https://doi.org/10.1364/AO.48.001473

Salinas, S. V., Chew, B.N., & Liew, S. C. (2009). Characterization of aerosol physical and optical properties from a combination of ground-based and hand-held sun-photometer data of singapore. *Conference Paper: International Geoscience and Remote Sensing Symposium*. Cape Town, South Africa: University of Cape Town. doi:10.1109/IGARSS.2009.5418136

Schmidt, L. S. (2001). Clouds in the balance. *Earth Observatory*. Retrieved from: https://earthobservatory.nasa.gov/

Smirnov, A., Holben, B. N., Eck, T. F., Dubovik, O., & Slutsker, I. (2000). Cloud-screening and quality control algorithms for the AERONET database. *Remote Sensing of Environment, 73*(3), 337-349. doi:10.1016/S0034-4257(00)00109-7

Smith, G. L., Priestley, K. J., Loeb, N. G., Wielicki, B. A., Charlock, T. P., Minnis, P., Rutan, D. A. (2011). Clouds and earth radiant energy system (CERES), a review: Past, present and future. *Advances in Space Research, 48*(2), 254-263. doi:10.1016/j.asr.2011.03.009

Soden, B. J., Wetherald, R. T., Stenchikov, G. L., Robock, A., (2002). Global Cooling after the Eruption of Mount Pinatubo: A Test of Climate Feedback by Water Vapor. *Science, 296* (5568), 727-730. Retrieved from http://www.jstor.org.libproxy1.nus.edu.sg/stable/3076586

Tan, C. (2017, January 21). Private car numbers fall to eight-year low. *The Straits Times*.

TODAY Online. (2015, October 20). PM2.5 levels hit 471 as haze situation worsens. *TODAY*. Retrieved March 27, 2017, from http://www.todayonline.com

Tomasi, C., Fuzzi, S., Kokhanovsky, A. (2017). Atmospheric Aerosols: Life Cycles and Effects on Air Quality and Climate (1st. ed.). Weinheim: Wiley-VCH. doi: http://dx.doi.org/10.1002/9783527336449

Velasco, E., & Roth, M. (2012). Review of Singapore's air quality and greenhouse gas emissions: current situation and opportunities. *Journal of the Air & Waste Management Association, 62*(6), 625. doi:10.1080/10962247.2012.666513

Yap, S. (2015, September 20). *Shanmugam: "Only so much" Singapore can do to help fight haze.* Retrieved from http://news.asiaone.com/news/singapore/shanmugam-only-so-much-singapore-can-do-help-fight-haze